

电压调制 ZnO 紫外探测器光响应截止波长的研究

段雨晗¹, 丛明煜^{1*}, 蒋大勇², 梁庆成²

¹ 哈尔滨工业大学空间光学工程研究中心, 黑龙江 哈尔滨 150001;

² 长春理工大学材料科学与工程学院, 吉林 长春 130022

摘要 通过射频磁控溅射技术, 成功制备了具有金属-半导体-金属(MSM)结构的ZnO紫外光电探测器。研究了外加偏压对探测器响应度和截止波长的影响。随着偏压的增大, 器件的响应度逐渐增加并且趋于饱和, 探测器的响应截止波长红移了12 nm。这是电场引起的耗尽层的展宽以及带隙倾斜造成的。提出了一种利用外加偏压控制探测器截止波长的有效方法, 该方法对紫外光电探测器的进一步研究和应用具有重要意义。

关键词 探测器; 光电探测器; 氧化锌; 金属-半导体-金属结构; 响应度; 截止波长; 红移

中图分类号 O472

文献标志码 A

doi: 10.3788/AOS202040.2004001

Spectral Response Cutoff Wavelength of ZnO Ultraviolet Photodetector Modulated by Bias Voltage

Duan Yuhan¹, Cong Mingyu^{1*}, Jiang Dayong², Liang Qingcheng²

¹ Research Center for Space Optical Engineering, Harbin Institute of Technology,
Harbin, Heilongjiang 150001, China;

² School of Materials Science and Engineering, Changchun University of Science and Technology,
Changchun, Jilin 130022, China

Abstract A ZnO ultraviolet photodetector with a metal-semiconductor-metal (MSM) structure was successfully prepared by the radio frequency magnetron sputtering technology. The bias voltage dependence of the responsivity and cutoff wavelength of the detector is studied. With the increase of bias voltage, the responsivity of the detector gradually increases and tends to saturate and the response cutoff wavelength of the detector is redshifted by 12 nm. This is attributed to the broadening of the depletion layer and the tilt of the bandgap caused by the field. In this work, an effective method is proposed to control the cutoff wavelength of the detector by an external bias voltage, which is of great significance to the further investigation and application of ultraviolet photodetectors.

Key words detector; photodetector; ZnO; metal-semiconductor-metal structure; responsivity; cutoff wavelength; redshift

OCIS codes 040.5160; 040.7190; 160.6000; 160.1890

1 引言

近年来, 紫外光电探测器因其在工业、军事、生物和环境等领域的广泛应用而受到越来越多的关注^[1-5]。在材料科学中, ZnO 作为一种半导体材料, 具有 3.37 eV 的带隙宽度, 60 meV 的激子束缚能^[6-8]以及较高的电子迁移率。ZnO 作为一种理想的短波长光电器件材料, 在激光二极管、发光二极管和紫外光电探测器等领域具有巨大的应用潜力^[9-13]。

金属-半导体-金属(MSM)结构可以看成是由两个背靠背接触的肖特基构成的。在这种结构中, 肖特基势垒可收集半导体薄膜中的光生载流子, 该收集分为平行于薄膜表面的横向收集和纵向收集。MSM 结构因其不需要制备 p 型材料, 制备工艺相对简单, 已经成为制备 ZnO 基紫外光电探测器的理想结构^[14]。众所周知, MSM 结构的肖特基光电探测器需要在外加偏压的条件下才能工作, 电压的施加不可避免地会影响器件的性能。当对探测器施加

收稿日期: 2020-05-27; 修回日期: 2020-06-27; 录用日期: 2020-07-06

基金项目: 国家自然科学基金(61774023)、吉林省教育厅“十三五”科研项目(JJKH20190587KJ)、吉林省科技发展计划项目(20190101008JH, 20200403048SF)

* E-mail: myconghit@126.com

外加偏压时,探测器截止波长可能会向长波长方向移动,即发生红移。这一现象可应用于电光调制、光开关、集成光学及探测器防护等高新技术领域中^[15]。目前,有许多关于探测器响应截止波长红移现象的研究。2002年,Zhang等^[16]发现在GaN/AlGaN量子阱中,多量子阱(MQWs)中的极化感应电场导致器件发生了4 nm红移。2003年,Teke等^[17]在GaN/AlGaN中,发现了MQWs中由极化感应电场引起的截止波长红移现象。然而,关于ZnO光电探测器中外加偏压与响应度之间的关系,特别是与截止波长之间关系的研究鲜有报道。2004年,Ozbay等^[18]发现,AlGaN日盲光探测器的截止波长随偏压发生了红移(266~274 nm)。由于红移现象的存在,可以利用外加偏压来控制探测器的截止波长,这对于拓宽紫外光电探测器的应用范围具有重要意义。然而,目前红移现象的机制尚不清楚。本文利用射频磁控溅射技术在蓝宝石(Al_2O_3)衬底上制备了ZnO薄膜。采用传统紫外曝光和湿法刻蚀方法制备了具有MSM结构的ZnO紫外光电探测器。在此基础上研究了外加偏压对探测器响应度和响应截止波长的影响,并对其物理机制进行了深入的分析。

2 实 验

2.1 ZnO 紫外光电探测器的制备

采用高纯度ZnO陶瓷靶材,利用射频磁控溅射技术在清洗过的 Al_2O_3 衬底上沉积ZnO薄膜。分别用丙酮、无水乙醇和去离子水对 Al_2O_3 衬底进行清洗,10 min后吹干。溅射前,启动分子泵抽高真空使溅射腔压强达到 5×10^{-4} Pa,而后将氧气和氩气的混合气体作为工作气体引入真空室中,氧氩流量比控制为10:40。在整个溅射过程中,溅射压强、衬底温度和射频源功率分别保持为0.6 Pa、400 °C、150 W,溅射时间为3 h。采用直流溅射方法在制备的ZnO薄膜上沉积了Au膜。通过紫外曝光与湿法刻蚀方法将Au膜刻蚀为叉指电极,叉指长度为500 μm ,叉指宽度和叉指间距均为5 μm 。

2.2 表征与测试

使用Rigaku Ultima VI设备及铜K α 对ZnO薄膜进行X射线衍射分析(XRD)。吸收光谱分析所使用的设备为紫外分光光度计A PerkinElmer Lambda 950 UV/VIS。采用JEM-67101F发射扫描电子显微镜(SEM)对器件的断面层结构和形貌进行表征。采用Agilent B1500半导体参数分析仪

和16442A测试夹具测量了探测器在黑暗和紫外光照射下的电流-电压(I-V)特性。响应度测量采用Zolix DR800-CUST测试系统。所有测量均在室温条件下进行。

3 分析与讨论

$\text{Au}/\text{ZnO}/\text{Al}_2\text{O}_3$ 紫外光电探测器的结构示意图如图1所示。图2(a)展示了 Al_2O_3 和ZnO薄膜的XRD图谱。可以看出,ZnO薄膜具有两个尖锐的衍射峰,分别对应于ZnO的(002)和(004)面,表明制备的ZnO薄膜具有良好的结晶性,ZnO为纤锌矿结构,并且具有c轴择优取向。ZnO薄膜的吸收光谱如图2(b)所示,在380 nm处存在一个明显的吸收截止边。由于ZnO为直接带隙半导体,通过绘制出 $(\alpha h\nu)^2$ 与 $h\nu$ 的关系曲线^[19](h 为普朗克常数, ν 为光子频率, α 为吸收系数),得到ZnO薄膜的带隙宽度为3.37 eV,如图2(b)插图所示。该结果与XRD结果一致,这表明高质量的氧化锌薄膜制备成功。

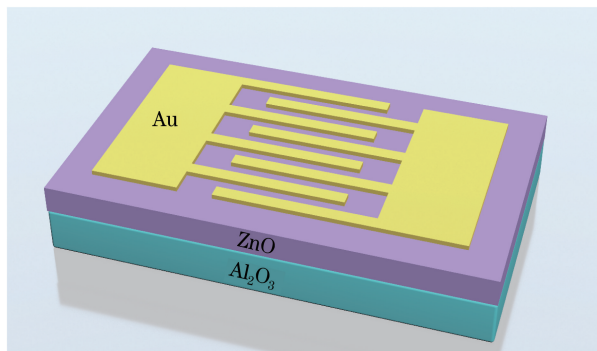


图1 ZnO紫外光电探测器的结构示意图

Fig. 1 Structural diagram of ZnO ultraviolet photodetector

图3(a)提供了具有MSM结构的ZnO紫外探测器叉指电极的SEM图片,可以看到器件的叉指电极整齐对称,叉指之间没有任何杂质。图3(b)为器件的断面层结构SEM图,ZnO和Au层厚度分别是550 nm和106 nm。ZnO薄膜与Au电极表面的SEM图分别如图3(c)、(d)所示。可以看到ZnO薄膜具有良好的平滑性和致密性,Au电极表面致密平整。平整致密的ZnO薄膜和Au电极有助于探测器接收不同角度入射的紫外光。

为了评估ZnO紫外光电探测器的性能,分别测试黑暗和365 nm光照条件下的I-V曲线,结果如图4所示。非线性的暗电流曲线表明该器件金属和半导体ZnO薄膜形成了非常好的肖特基接触。此外,器件表现出较小的暗电流,表明最低可检测光功

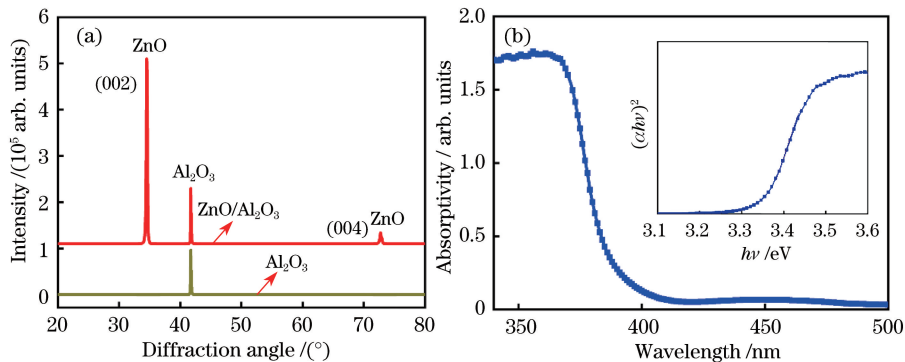


图 2 ZnO 薄膜的性能表征。(a) ZnO 薄膜和 Al₂O₃ 的 XRD 图; (b) ZnO 薄膜的紫外-可见吸收光谱, 插图为 (ahv)²-hv 图谱

Fig. 2 Performance characterization of ZnO film. (a) XRD spectra of ZnO film and Al₂O₃; (b) UV-visible absorption spectrum of ZnO film with (ahv)²-hv spectrum shown in inset

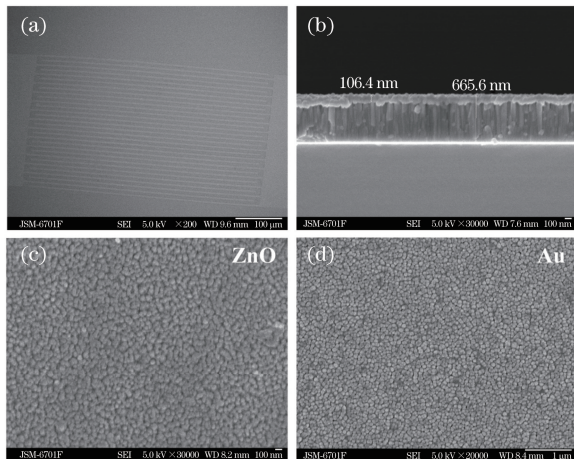


图 3 ZnO 紫外光电探测器的性能表征。(a) MSM 结构的 ZnO 紫外光电探测器的 SEM 图;(b) 器件的断面 SEM 图;(c) ZnO 薄膜的俯视 SEM 图;(d) Au 膜的俯视 SEM 图

Fig. 3 Performance characterization of ZnO ultraviolet photodetector. (a) SEM image of ZnO ultraviolet photodetector with MSM structure; (b) cross-sectional SEM image of device; (c) top view of SEM image of ZnO film; (d) top view of SEM image of Au film

率得到有效降低, 微弱光的检测能力得到提高。此外, 器件在 365 nm 紫外光照射下, 光电流增大, 并且光电流与暗电流之比约为 10⁴。

图 5(a)是 5~65 V 外加偏压下 ZnO 紫外光电探测器的光谱响应曲线。可以明显看到, 响应度随着外加偏压的增大而增大。为了清晰地展示响应度峰值的变化, 图 5(b)提供了器件的响应度峰值随外加偏压变化的拟合曲线。当外加偏压从 5 V 增加到 65 V 时, 响应度迅速增加, 而后增加缓慢, 进而趋于饱和。除此之外, 还发现一个有趣的现象, 当外加偏压增加时, 探测器截止边发生移动, 向长波长方向移

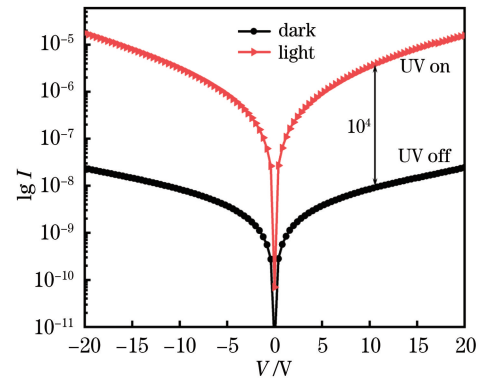


图 4 对数坐标下的 I-V 特性曲线

Fig. 4 I-V characteristic curves in logarithmic coordinate system. In order to facilitate comparison, all response degrees were normalized. As shown in Fig. 5(c), the response degree was increased with the increase of external bias voltage. At the same time, the physical mechanism of the response degree increase with the increase of external bias voltage was revealed. Figure 5(d) provides the enlarged image of the response edge of the detector. The inset shows the change of the response edge with the increase of the external bias voltage. When the external bias voltage increased from 5 V to 65 V, the response degree increased rapidly and then increased slowly, finally reaching saturation. In addition, it was found that when the external bias voltage increased, the response edge of the detector moved, shifting to the long wavelength direction. To understand the phenomenon of the response degree increasing with the increase of the external bias voltage and then saturating, Figure 6 gives the energy band diagram of the ZnO ultraviolet photodetector under an external bias voltage. In the diagram, E is energy, k is wave vector, E_c is conduction band bottom, E_f is Fermi level, and E_v is valence band top.

对于半导体而言, 在所施加的偏压不大的情况下, 当光子能量大于带隙能量的时候, 电子就会从价带顶跃迁到导带底, 如图 6(a)所示。随着偏压的增加, 电场强度增大^[20]。当半导体上施加有外电场时, 多数载流子即电子从负电极端流向正电极端, 并在外电路中产生电流。这种作用在能带图上就表现为能带的倾斜, 如图 6(b)所示。导带底对应的能级可以认为是电子的电势能, 负电极端的势能高, 正电

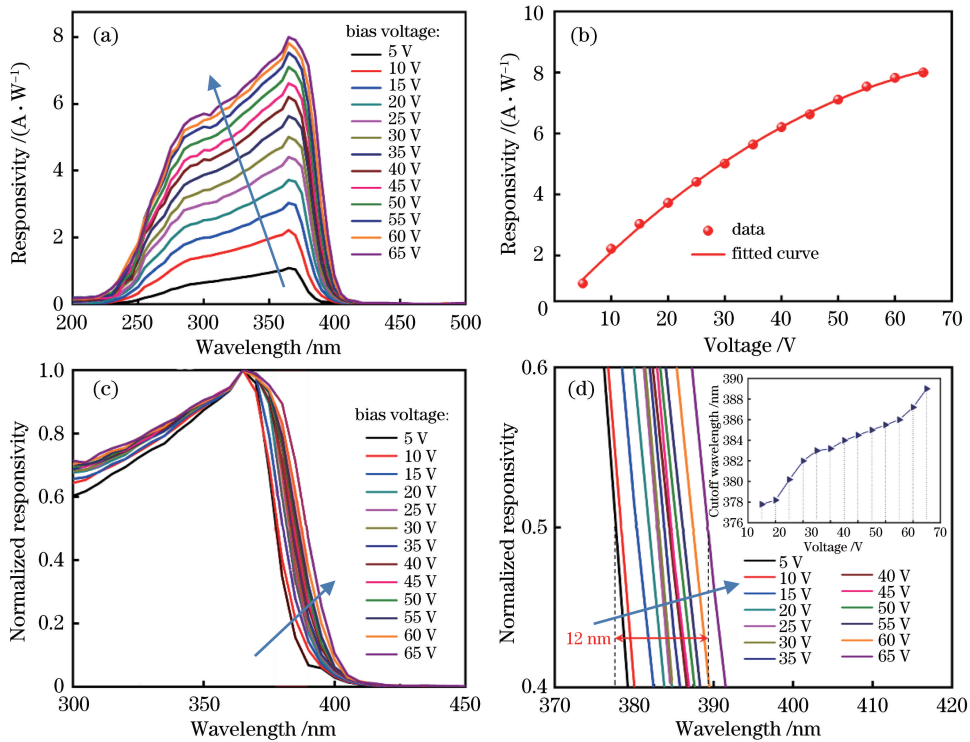


图 5 ZnO 紫外光电探测器的光谱响应曲线。(a) 不同外加偏压下的 ZnO 光电探测器的响应度;(b) 响应度峰值与外加偏压的关系;(c) ZnO 光电探测器的归一化响应度;(d) 响应截止边的放大图,插图为响应截止边与外加偏压的关系

Fig. 5 Spectral responsivity curves of ZnO ultraviolet photodetector. (a) Responsivity of ZnO ultraviolet photodetector with different external bias voltages; (b) peak responsivity versus external bias voltage; (c) normalized responsivity of ZnO ultraviolet photodetector; (d) enlarged diagram of response cutoff wavelength with response cutoff wavelength versus bias voltage shown in inset

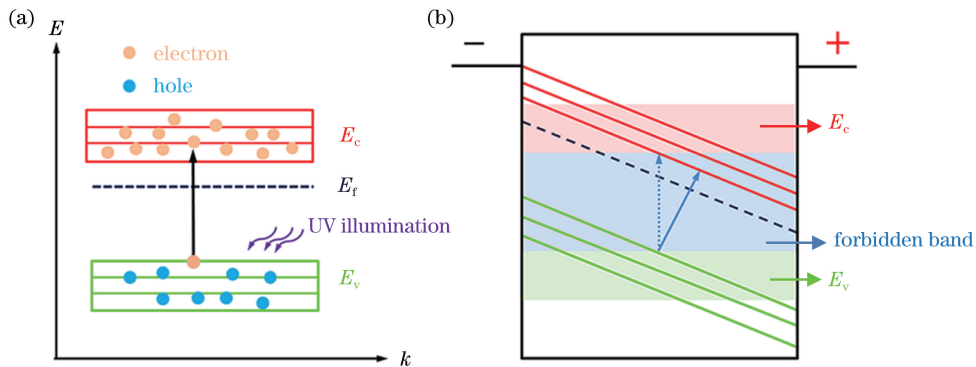


图 6 半导体电子能带示意图。(a) 半导体能带图;(b) 电场作用下的能带倾斜图
Fig. 6 Schematic of semiconductor electron energy band. (a) Semiconductor energy band diagram;
(b) energy band tilt diagram under action of electrical field

极端的势能低,从而外电场使得能带发生倾斜。由于 MSM 结构是双肖特基型的背靠背结构,当偏压增大时,带隙倾斜程度增大,同时电极两侧两个耗尽层的总宽度会逐渐增加,直至电极两边的耗尽层相互接触。随着偏压的继续增大,带隙继续倾斜,并且电极一侧的耗尽层宽度增加为与电极间距相等,另一侧耗尽层宽度为 0。此时响应度趋于饱和。由于带隙倾斜,价带电子跃迁到导带所需要的光子能量

可以小于禁带宽度,价带电子跃迁到导带的几率大大增加,有效能隙减小(光学带隙并未发生变化),从而响应截止边发生红移。

4 结 论

采用射频磁控溅射方法在 Al_2O_3 上成功设计并制备了具有 MSM 结构的 ZnO 紫外光电探测器。随着外加偏压从 5 V 增加到 65 V, 响应度逐渐升高

并趋于饱和，并且探测器截止波长从378 nm移动到390 nm，红移了12 nm。由于外加偏压的增加，耗尽层的宽度逐渐增加，带隙倾斜，有效带隙减小，从而响应度饱和，响应截止边发生红移现象。结果表明，在器件上施加偏压是调节探测器截止波长的有效途径，该方法对进一步研究和开发光电探测器具有重要意义。

参 考 文 献

- [1] Soci C, Zhang A, Xiang B, et al. ZnO nanowire UV photodetectors with high internal gain[J]. *Nano Letters*, 2007, 7(4): 1003-1009.
- [2] Kind H, Yan H, Messer B, et al. Nanowire ultraviolet photodetectors and optical switches [J]. *Advanced Materials*, 2002, 14(2): 158-160.
- [3] Pearton S J, Ren F, Wang Y L, et al. Recent advances in wide bandgap semiconductor biological and gas sensors [J]. *Progress in Materials Science*, 2010, 55(1): 1-59.
- [4] Zhang X M, Lu M Y, Zhang Y, et al. Fabrication of a high-brightness blue-light-emitting diode using a ZnO-nanowire array grown on p-GaN thin film [J]. *Advanced Materials*, 2009, 21(27): 2767-2770.
- [5] Hou Y N, Mei Z X, Liu Z L, et al. Mg_{0.55}Zn_{0.45}O solar-blind ultraviolet detector with high photoresponse performance and large internal gain[J]. *Applied Physics Letters*, 2011, 98(10): 103506.
- [6] Wang W, Zhang F C, Yan J F, et al. Synthesis and optical properties of nano-ZnO at low temperature [J]. *Laser & Optoelectronics Progress*, 2018, 55(7): 071603.
王魏, 张富春, 谭军锋, 等. 低温合成纳米氧化锌及其光学性能研究[J]. 激光与光电子学进展, 2018, 55(7): 071603.
- [7] Chen K J, Hung F Y, Chang S J, et al. Optoelectronic characteristics of UV photodetector based on ZnO nanowire thin films [J]. *Journal of Alloys and Compounds*, 2009, 479(1/2): 674-677.
- [8] Yan Z, Song Z T, Liu W L, et al. Optical and electrical properties of p-type zinc oxide thin films synthesized by ion beam assisted deposition[J]. *Thin Solid Films*, 2005, 492(1/2): 203-206.
- [9] Hu Y, Chen Y Q, Wu Y C, et al. Structural, defect and optical properties of ZnO films grown under various O₂/Ar gas ratios [J]. *Applied Surface Science*, 2009, 255(22): 9279-9284.
- [10] Minemoto T, Negami T, Nishiwaki S, et al. Preparation of Zn_{1-x}Mg_xO films by radio frequency magnetron sputtering [J]. *Thin Solid Films*, 2000, 372(1/2): 173-176.
- [11] Prepelita P, Medianu R, Sbarcea B, et al. The influence of using different substrates on the structural and optical characteristics of ZnO thin films [J]. *Applied Surface Science*, 2010, 256(6): 1807-1811.
- [12] Sans J A, Segura A, Mollar M, et al. Optical properties of thin films of ZnO prepared by pulsed laser deposition [J]. *Thin Solid Films*, 2004, 453/454: 251-255.
- [13] Yang P F, Wen H C, Jian S R, et al. Characteristics of ZnO thin films prepared by radio frequency magnetron sputtering [J]. *Microelectronics Reliability*, 2008, 48(3): 389-394.
- [14] Baccarani G, Calzolari P, Graffi S. Current transport in MSM devices [J]. *Journal of Applied Physics*, 1974, 45(1): 341-344.
- [15] Li Z D, Ye Y T, Wu Y F, et al. A method for characterizing effective intensity of Franz-Keldysh effect in (HgCd)Te detectors [J]. *Journal of Infrared & Millimeter Waves*, 2001, 20(5): 353-355.
李正东, 叶玉堂, 吴云峰, 等. (HgCd)Te 探测器 Franz-Keldysh 效应有效强度的一种表征方法 [J]. 红外与毫米波学报, 2001, 20(5): 353-355.
- [16] Zhang S L, Wang W, Yun F, et al. Backilluminated ultraviolet photodetector based on GaN/AlGaN multiple quantum wells [J]. *Applied Physics Letters*, 2002, 81(24): 4628-4630.
- [17] Teke A, Dogan S, Yun F, et al. GaN/AlGaN back-illuminated multiple-quantum-well Schottky barrier ultraviolet photodetectors [J]. *Solid-State Electronics*, 2003, 47(8): 1401-1408.
- [18] Ozbay E, Biyikli N, Kimukin I, et al. High-performance solar-blind photodetectors based on Al_xGa_{1-x}N heterostructures [J]. *IEEE Journal of Selected Topics in Quantum Electronics*, 2004, 10(4): 742-751.
- [19] Hagfeldt A, Graetzel M. Light-induced redox reactions in nanocrystalline systems [J]. *Chemical Reviews*, 1995, 95(1): 49-68.
- [20] Zhao M, Wang X, Yang G, et al. Bias induced cutoff redshift of photocurrent in ZnO ultraviolet photodetectors [J]. *Applied Surface Science*, 2015, 359: 432-434.